Elastic and Inelastic Scattering of 187-Mev Electrons from Carbon-12†

JEROME H. FREGEAU*‡
Department of Physics and High-Energy Physics Laboratory, Stanford University, Stanford, California
(Received June 19, 1956)

The scattering of 187-Mev electrons from C^{12}, reported previously, has been extended to 138°. It has been possible to separate the elastic scattering from the inelastic scattering and to resolve the inelastic groups from the 4.43-, 7.65-, and 9.61-Mev nuclear levels. "Absolute" values were obtained by comparing the scattering from carbon with the scattering from hydrogen and computing the proton cross section. The angular distribution of the elastically-scattered electrons falls off more steeply than the angular distribution of the inelastically-scattered electrons. Analysis of the data, using the Born approximation, shows that the root-mean-square radius of C^{12} (corrected for breakdown of the Born approximation) is $(2.37\pm0.05)\times10^{-13}$ cm with a surface thickness of $(2.0\pm0.4)\times10^{-13}$ cm. The corresponding value of r_0, the "classical" radius parameter, is $(1.33\pm0.02)\times10^{-13}$ cm which is larger than that found from electron-scattering measurements for the heavy nuclei and is in agreement with the trend for light nuclei. The scattering from the 4.43-Mev and 7.65-Mev levels is larger than that predicted by some shell-model calculations. The transition from the ground state to the 9.61-Mev level appears to be either quadrupole or electric monopole, which gives a spin and parity assignment of either 2^+ or 0^+.

I. INTRODUCTION

IN a previous paper,[1] the scattering of high-energy electrons from C^{12} at angles up to 90° was reported. This work has been extended to 138° at 187 Mev and the elastic-scattering results have been analyzed in terms of the first Born approximation. The large-angle scattering deviates from point-charge scattering by factors of one thousand or more and provides a much more rigorous test of nuclear models than the earlier data. Measurements of the cross sections for inelastic scattering with excitation of the 4.43-Mev, 7.65-Mev, and 9.61-Mev levels have also been made. At angles of 100° or larger at 187 Mev, the inelastic 4.43-Mev scattering is larger than the elastic scattering, as is the 9.61-Mev scattering, at angles greater than 110°.

A number of authors, using several different nuclear models, have attempted to calculate the elastic and 4.43-Mev level scattering cross sections,[2,3] and the transition matrix elements between the ground state of C^{12} and the 7.65-Mev level.[4–6] While the elastic scattering data may be fitted quite well, the inelastic scattering data disagree with all predictions by at least a factor of two. Collective models give predictions which are too large, and independent-particle models give predictions which are too small.

II. EXPERIMENTAL PROCEDURE AND RESULTS

The experimental apparatus used in this work has been described in several previous papers.[1,7–9] The incoming energy spectrum and the spectrometer energy resolution were set at 0.2% for angles up to 90° and 0.5% for larger angles where cross sections are much smaller. At the large angles, the bremsstrahlung tail of the elastic peak does not interfere with inelastic measurements since the ratio of inelastic to elastic scattering is large. This allows poorer energy resolution to be used.

For angles of 100° and larger, the area under the elastic peak was compared with the area under the elastic peak at 70° which was taken in the same run. Corrections were made for changes in target thickness as the target was rotated (the normal to the target bisected the scattering angle) and for changes in absolute magnet dispersion with outgoing-electron energy (the relative dispersion is constant). Since the

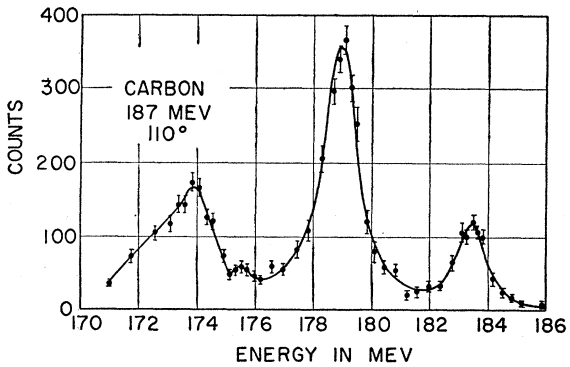

FIG. 1. Scattering at 187 Mev at an angle of 110°. This is a composite of two runs.

† This work was done in partial fulfillment of the requirements of the degree of Doctor of Philosophy at Stanford University. It was supported jointly by the Office of Naval Research and the U. S. Atomic Energy Commission, and by the U. S. Air Force through the Office of Scientific Research of the Air Research and Development Command. The work was aided by a grant from the Research Corporation.

* International Business Machine Fellow for the year 1954–1955.
‡ Now at the Department of Physics, University of Michigan, Ann Arbor, Michigan.

[1] J. H. Fregeau and R. Hofstadter, Phys. Rev. **99**, 1503 (1955).
[2] D. G. Ravenhall (to be published).
[3] G. Morpurgo, Nuovo cimento **3**, 430 (1956).
[4] L. I. Schiff, Phys. Rev. **96**, 765 (1954).
[5] L. I. Schiff, Phys. Rev. **98**, 1281 (1955).
[6] B. Sherman and D. G. Ravenhall (to be published).
[7] Hofstadter, Fechter, and McIntyre, Phys. Rev. **92**, 978 (1953).
[8] Hofstadter, Hahn, Knudsen, and McIntyre, Phys. Rev. **95**, 512 (1954).
[9] J. A. McIntyre and R. Hofstadter, Phys. Rev. **98**, 158 (1955).

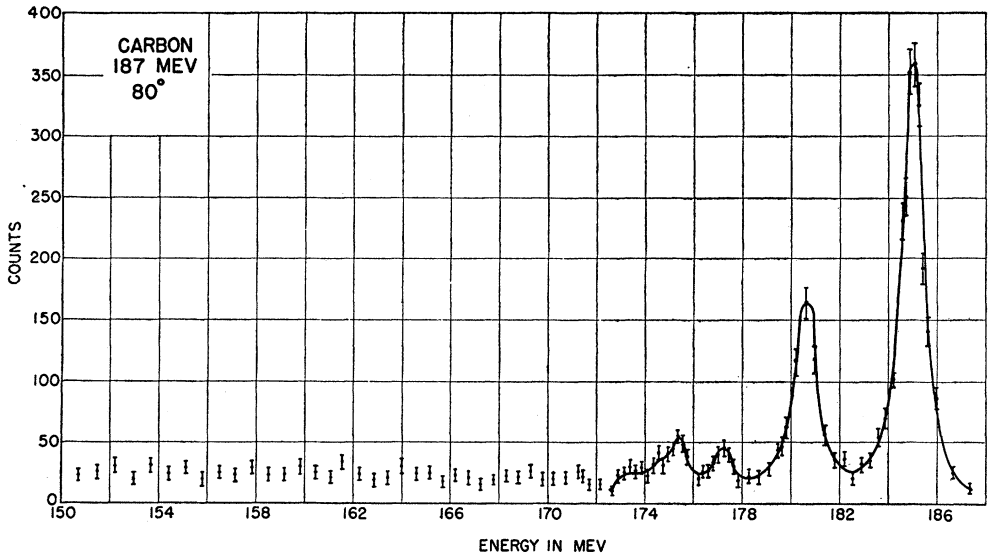

FIG. 2. Scattering at 187 Mev at an angle of 80°.

absolute value of the 70° elastic cross section at 187 Mev had been found by comparison with elastic scattering from hydrogen and a computation of the hydrogen cross section,[1] the values of the cross sections at the larger angles could be determined. A similar treatment was given to the 4.43-Mev cross section. The cross sections for the 7.65-Mev and 9.61-Mev peaks were found by comparing the heights of these peaks, after subtraction of the bremsstrahlung tail of the elastic and 4.43-Mev peaks, with the height of the 4.43-Mev peak.

Figure 1, which is a composite of two runs, shows the elastic and inelastic scattering at 110° and 187 Mev. The peak at 183.4 Mev is due to elastic scattering; that at 179.0 Mev, to the 4.43-Mev level; that at about 175.6 Mev, to the 7.65-Mev level; and that at 174 Mev, to the 9.61-Mev level. The broadening of the low-energy edge of the 9.61-Mev peak is caused by scattering from the higher energy levels in C^{12}, which are too close together to be resolved.

At 80°, scattering with excitation up to about 34 Mev was investigated. Figure 2 shows the results of a single run with the elastic peak at 185 Mev and the first three inelastic peaks at 180.5 Mev, 177.3 Mev, and 175.4 Mev. Above 10-Mev excitation, the known energy levels are too close together to be resolved unless excitation of a particular level occurs with a much higher probability than excitation of neighboring levels. This clearly is not the case at 85°. In particular, the 15.2-Mev level does not show strong excitation, contrary to what might be expected from gamma-ray studies.[10]

A correction for the use of thick targets was found to be necessary. This effect arises from two sources, radiation by the electron of more than 1.5 Mev while in the target, and geometrical effects due to finite beam-spot size and finite magnet aperture. The former has been calculated by Bethe and Heitler.[11] The latter was determined empirically by measuring the elastic scattering from four targets of different thicknesses at 90° and two targets at 110°.

At angles less than 90°, the effect was small since variation of target thickness with angle was small and only variations with angle were significant. Above 100° this effect becomes quite important, being 12% at 120° and 24% at 138°. The thick-target radiation corrections at these angles were 9% and 17%, respectively. The geometric correction is not known accurately, and was larger than the 6% predicted by rough calculations based on the characteristics of the analyzing magnet, its vacuum chamber, the magnet input aperture, the target size and position, and the beam-spot size. However, the uncertainty in this correction would not change cross sections by more than a few percent in the region from 100° to 138°. Since the cross sections drop by a factor of at least four for inelastic scattering between 120° and 138°, and by a factor of about twenty for elastic scattering in the same region, and since statistical errors are large because counting rates were low, an uncertainty of this size is not important. The possible error at 90° or less was negligible.

Another correction of much less importance was due to the vertical opening of the spectrometer input aperture. The actual angle of scattering for electrons which passed through the top or bottom of this opening

[10] Cohen, Moyer, Shaw, and Waddell, Phys. Rev. **96**, 714 (1954); Rasmussen, Rees, Sampson, and Wall, Phys. Rev. **96**, 812 (1954); Waddell, Shaw, Cohen, and Moyer, Phys. Rev. **96**, 858(A) (1954); Fuller, Hayward, and Svantesson, Bull. Am. Phys. Soc. Ser. II, **1**, 21 (1956).

[11] H. A. Bethe and J. Ashkin, in *Experimental Nuclear Physics*, edited by E. Segrè (John Wiley and Sons, Inc., New York, 1953), Vol. I, p. 272.

TABLE I. Results. Differential cross sections in the laboratory system in units of 10^{-30} cm²/sterad for angles of 90° or less and in units of 10^{-33} cm²/sterad for angles greater than 90°. Errors are statistical only.

E	θ_{lab}	Elastic	4.43 Mev	7.65 Mev	9.61 Mev
187 Mev	35°	280 ±14.0	2.32 ±0.28	1.04 ±0.22	0.481±0.190
	45°	68.7 ± 2.8	1.41 ±0.16 1.13 ±0.19	0.440±0.083 0.240±0.096	0.185±0.087
	50°	36.3 ± 1.5	1.46 ±0.16 1.12 ±0.23	0.490±0.069 0.391±0.090	0.391±0.078 0.243±0.070
	60°	9.53 ± 0.38	0.724±0.087 0.834±0.170	0.182±0.027 0.146±0.035	0.143±0.024 0.122±0.031
	70°	2.80 ± 0.11	0.514±0.051 0.498±0.065	0.095±0.017 0.082±0.027	0.131±0.020 0.137±0.036
	80°	0.748± 0.030	0.300±0.036 0.263±0.026	0.053±0.017 0.040±0.011	0.079±0.014 0.072±0.013
	90°	0.213± 0.015	0.168±0.019 0.192±0.023	0.014±0.006 0.022±0.006	0.062±0.011 0.046±0.011
	100°	46.6 ± 8.4 45.2 ± 2.7	83.6 ±9.2 65.1 ±4.6	...	...
	110°	9.84 ± 0.69	33.9 ±2.0 35.8 ±2.1	1.86 ±0.93	12.6 ±1.6
	120°	2.45 ± 0.30 1.90 ± 0.15	17.3 ±1.21		
	130°	0.569± 0.069	8.83 ±0.80	...	...
	138°	0.065< 0.100	4.29 ±0.30	<0.305	2.78 $^{+0.56}_{-1.11}$
150 Mev	70°	9.77 ± 0.39	0.610±0.067	0.148±0.025	0.103±0.021
	80°	3.23 ± 0.13	0.323±0.042	0.034±0.017	0.081±0.021
	90°	1.20 ± 0.05	0.170±0.019	0.043±0.011	0.047±0.011
80 Mev	90°	3.48 ± 0.18	0.182±0.040	...	...

differed by a small amount from the angle of scattering of electrons which passed through the center of the slit. This difference changes the mean angle of scattering by an amount $\frac{1}{2}\epsilon^2 \cot\theta$ from the nominal scattering angle θ, where ϵ is half the angle subtended at the target by the vertical opening. In this experiment ϵ was 0.057 radian and the correction was 7′ at 35°, 0′ at 90°, and −5′ at 138°. This correction has been made but has so little effect that it could have been neglected. Helm[12] has shown that, for experiments of this type and with this equipment, corrections to the cross sections due to finite angular and energy resolution are negligible in the region where a Born approximation is valid (see next section). The effects of plural and multiple scattering were negligible.

The results of this experiment are given in Table I. Because of the thick-target correction, the values differ by 1% at 35°, 0% at 50°, 3% at 70°, and 6% at 90° from those previously presented. The 187-Mev results are summarized in Fig. 3. This figure shows the angular distribution of the elastic scattering (Curve A) and the distributions of the inelastic scattering corresponding to the first three excited states of C^{12} (Curve B, 4.43 Mev; Curve C, 7.65 Mev; Curve D, 9.61 Mev). At 138°, only upper limits have been placed on the elastic and 7.65-Mev scattering since these cross sections were too small to be measured.

On all of the graphs and in the table of results, only errors due to counting statistics are shown. These are a combination of standard deviations of all data used in determining a given cross section. Other errors effecting the relative values of the angular distributions are believed to be much less than the statistical errors. Since the absolute values depend upon the hydrogen-calibration procedure,[1] they are not considered as accurate as the relative values. An error incalibration would change all absolute values by the same fraction. The error in this scaling factor is believed to be not more than 10%. Commerical graphite (National Carbon Company, grade AVC) was used as the target. According to the manufacturers, this grade of graphite has an ash content of less than 0.1%. No indications of effects due to impurities were found in the scattering runs.

III. ANALYSIS

In analyzing the results, it is necessary to set up a more or less detailed model of the nucleus and to

[12] R. H. Helm, Stanford University High-Energy Physics Laboratory Report No. 40 (unpublished), and to be published.

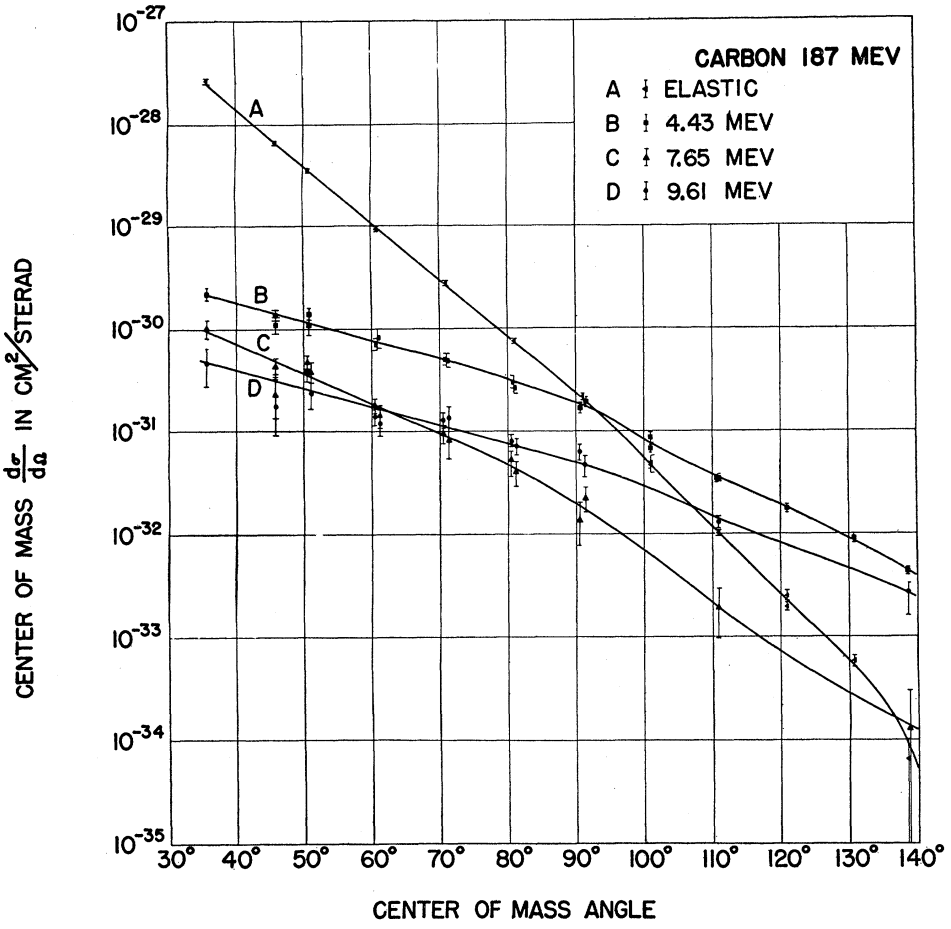

FIG. 3. Elastic and inelastic angular distributions at 187 Mev. The absolute cross sections have been obtained by the proton-normalization method discussed in the text.

deduce, from the model, cross sections which can be compared with experiment. One of the simplest and least detailed types of model is a continuous charge distribution in the nucleus, which has been used to analyze previous high-energy electron scattering measurements.[1,7–9,12–15] This model will be used in discussing the present experiment. In most cases, no attempt has been made to predict this charge distribution from nuclear theory. Recently, however, Ravenhall[2] has made shell-model calculations of the C^{12} charge distributions for several different types of nuclear potential wells. Morpurgo[3] has made similar calculations using a harmonic oscillator well, and Visscher and Ferrell[16] have calculated root-mean-square radii for nuclei between lithium and oxygen based on shell model theory. Carbon inelastic scattering calculations have been made by Schiff[4,5] using both the shell model and collective models, and by Ravenhall,[12] Morpurgo,[3] and others[17,18] using the shell model.

In the present analysis, the Born approximation is used, rather than the accurate phase-shift methods of Yennie *et al.*,[15] for reasons of simplicity. The validity criterion is that $Z/137 \ll 1$ where Z is the atomic number of the nucleus. For carbon, $Z/137$ is about 0.05. Yennie *et al.*[15] have shown that, for monotonic angular distributions, the Born approximation is good for values of the momentum transfer parameter q up to about 0.9 of the q value for which the theoretical cross section goes to zero. In this experiment, the approximation is good up to 120°, but cannot be trusted for larger angles. The root-mean-square radii and surface thicknesses found from these calculations are larger than the values which would be found from exact calculations since the change of the electron wave number while the electron is in the nucleus is ingored. An estimate[2] of this change, assuming a uniform charge distribution of radius R, gives a reduction in rms radius and surface thickness by the factor $(1+3\alpha Z/2kR)^{-1}$, where Z is the atomic number of the nucleus, $\alpha=1/137$ is the fine

[13] Hahn, Ravenhall, and Hofstadter, Phys. Rev. **101**, 1131 (1956).
[14] L. I. Schiff, Phys. Rev. **92**, 988 (1953).
[15] Yennie, Ravenhall, and Wilson, Phys. Rev. **92**, 1325 (1953); **95**, 500 (1954).
[16] W. M. Visscher and R. A. Ferrell, Bull. Am. Phys. Soc. Ser. II, **1**, 17 (1956).
[17] J. P. Elliott, Phys. Rev. **101**, 1212 (1956).
[18] P. J. Redmond, Phys. Rev. **101**, 751 (1956).

structure constant, and k is the momentum of the incoming electron measured in wave numbers. This reduction is about 1.3% for carbon. Phase-shift calculations have been made by Ravenhall[2] for a modified Gaussian charge distribution derived from shell-model theory. These calculations are valid up to 90° and show a deviation from the Born-approximation result at 90° of about 6%. This would give a radius about 1.4% smaller than that found from the Born approximation, in agreement with the preceding discussion. It is believed, therefore, that all radii determined from the Born-approximation analysis of this experiment should be decreased by about 1.4%.

The Born-approximation result for high-energy electron scattering may be written

$$d\sigma/d\Omega=(d\sigma/d\Omega)_{\text{point}}|F|^2, \tag{1}$$

where $(d\sigma/d\Omega)_{\text{point}}$ is the differential scattering cross section of a point charge. The nuclear form factor F is

$$F(q)=\int\rho(\mathbf{r})e^{i\mathbf{q}\cdot\mathbf{r}}d^3\mathbf{r}, \tag{2}$$

where q is the change of momentum of the electron in the scattering process measured in wave numbers and $\rho(\mathbf{r})$ is the nuclear charge distribution, normalized so that $\int\rho(\mathbf{r})d^3\mathbf{r}=1$. Because, as Hahn *et al.*[13] have shown, at these energies only a radius and a surface thickness can be determined, spherically symmetric charge distributions are assumed. The formulas then reduce to

$$F(q)=\frac{4\pi}{q}\int_0^\infty\rho(r)(\sin qr)rdr, \tag{3}$$

$$4\pi\int_0^\infty\rho(r)r^2dr=1, \tag{4}$$

$$q=(2E/\hbar c)\sin(\theta/2), \tag{5}$$

where $\hbar$ is Planck's constant divided by 2π, c is the velocity of light, E is the electron energy, and θ is the scattering angle. The point-charge cross section in the Born approximation is

$$(d\sigma/d\Omega)_{\text{point}}=\left(\frac{Ze}{2pv}\right)^2\frac{\cos^2(\theta/2)}{\sin^4(\theta/2)}\propto\frac{E^2\cos^2(\theta/2)}{q^4}, \tag{6}$$

where Ze is the nuclear charge, e is the charge of the electron, and p and v are the momentum and velocity of the electron, respectively. Since this experiment was done in the extreme relativistic region, pv is almost exactly approximated by E. The root-mean-square radius is

$$\langle r^2\rangle^{\frac{1}{2}}=\left|\int r^2\rho(\mathbf{r})d^3\mathbf{r}\right|^{\frac{1}{2}}, \tag{7}$$

where $p(\mathbf{r})$ is normalized by Eq. (4).

A. Elastic Scattering

The differences in the scattering cross sections found from different charge distributions occur only in the form factors. Since it was more convenient to compare calculated form factors with the experimentally determined form factor than to compare the cross sections themselves, the former procedure was adopted. The square of the experimental form factor for a given angle was found by transforming the cross section from the laboratory frame of reference to the center-of-mass frame and dividing by the point-charge cross section for the angle in the center-of-mass frame corresponding to the experimental angle. The square root of this may then be compared with the calculated form factor.

The method of comparing theory and experiment is that suggested by Schiff.[14] Since the absolute values of the experimental cross sections are not known as accurately as the relative values, it is necessary to introduce a scale factor λ. An estimate of the permissible deviation of the radial parameter a from the optimum value may be made. This was usually about 2%.

Schiff[14] has suggested several possible charge distributions which, while not necessarily realistic, are easily analyzed by this method. These, with their form factors and root-mean-square radii are

$$\begin{aligned}(\text{uniform})\rho(r)&=\rho_0,\quad r<a,\\&=0,\quad r>a,\\F(q)&=[3/(qa)^3](\sin qa-qa\cos qa),\\\langle r^2\rangle^{\frac{1}{2}}&=a\sqrt{\tfrac{3}{5}};\end{aligned} \tag{8}$$

$$\begin{aligned}(\text{Gaussian})\rho(r)&=\rho_0\exp(-r^2/a^2),\\F(q)&=\exp(-q^2a^2/4),\\\langle r^2\rangle^{\frac{1}{2}}&=a\sqrt{\tfrac{3}{2}};\end{aligned} \tag{9}$$

$$\begin{aligned}(\text{exponential})\rho(r)&=\rho_0e^{-r/a},\\F(q)&=(1+a^2q^2)^{-2},\\\langle r^2\rangle^{\frac{1}{2}}&=a\sqrt{12};\end{aligned} \tag{10}$$

$$\begin{aligned}(\text{modified exponential})\rho(r)&=\rho_0(1+r/a)e^{-r/a},\\F(q)&=(1+q^2a^2)^{-3},\\\langle r^2\rangle^{\frac{1}{2}}&=a\sqrt{18}\end{aligned} \tag{11}$$

$$\begin{aligned}(\text{inverse power})\rho(r)&=\rho_0(1+r^2/a^2)^{-2},\\F(q)&=e^{-qa},\\\langle r^2\rangle^{\frac{1}{2}}&=\infty.\end{aligned} \tag{12}$$

These squares of these form factors, using the optimum radial values and scaled to fit the experimental values, are plotted logarithmically against q in Fig. 4. The experimental results are also shown. None of these fit, and a charge distribution lying between the uniform and the Gaussian models appears indicated.

Shell model calculations by Ravenhall[2] and Morpurgo,[3] using an infinite harmonic well for the nuclear potential, have given the following charge distribution:

$$\rho(r)=\rho_0(1+4r^2/3a^2)\exp(-r^2/a^2). \tag{13}$$

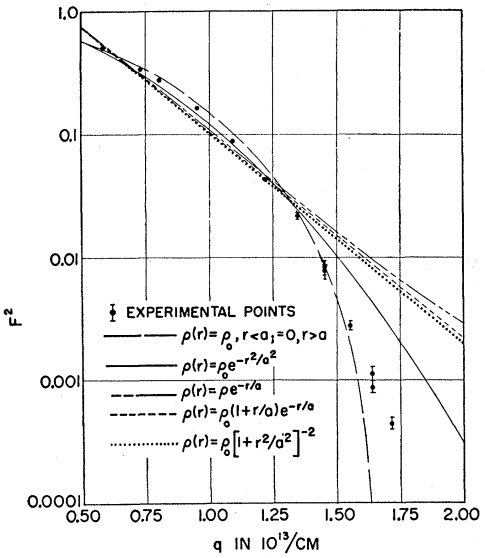

FIG. 4. Comparison of the square of the experimental form factor with the squares of the form factors for several models. The curves have been adjusted to give the best fit.

This suggested trying the family of charge distributions

$$\rho(r)=\rho_0(1+\alpha r^2)\exp(-r^2/a^2)$$

(modified Gaussian)

$$F(q)=\left(1-\frac{\alpha q^2a^2}{2(2+3\alpha)}\right)\exp(-q^2a^2/4)$$
$$\langle r^2\rangle^{\frac{1}{2}}=\left[\frac{3(2+5\alpha)}{2(2+3\alpha)}a\right]^{\frac{1}{2}}, \tag{14}$$

where α as well as a and the scale factor are free parameters.

Graphical analysis showed that extremely good fits could be obtained between this form factor and the experimental form factor for values of α between 1 and 2. A least-squares analysis of the type used by Hahn *et al.*[13] was made for $\alpha=1, 4/3$, and 2. For any given value of α, a value of a differing by 1% from the optimum gives only 60% as large a probability of fit as the optimum value, but several combinations of α and a give high probability. The best fit is obtained with $\alpha=4/3$, in agreement with the shell-model calculations. In this case, the absolute values of the cross sections, as determined by this experiment, agree with theory within about 1%. This is better than might be expected considering the possible errors in the experimental values. The maximum probability of fit for $\alpha=1$ is about 80% of that for $\alpha=4/3$ and for $\alpha=2$ is only 60%. In these cases, the absolute values disagree by about 7%. This is not considered unreasonable.

Comparison of theory with experiment for these three values of α, using the optimum values of a and λ, the scale factor, is shown in Fig. 5 where the square of the form factor is plotted logarithmically against scattering angle. In order to show detail, the curves have been broken into two parts. The numerical values of F^2 for the left curve are given at the left edge, and those for the right curve, at the right edge. All three models fit the experimental points well, with $\alpha=4/3$ being slightly better than the other two. Beyond about 120°, the Born approximation is not expected to be valid so that this region must be ignored in determining the fit.

Another family of models suggested by Ravenhall[19] is (modified trigonometric)

$$\rho(r)=\rho_0(1+\alpha\pi^2r^2/a^2)\frac{\sin^2(\pi r/a)}{\pi^2r^2/a^2},$$
$$F(q)=\frac{1}{[1+\alpha(\pi^2/3-\frac{1}{2})]qa}\{\mathrm{Si}(qa)-\tfrac{1}{2}\,\mathrm{Si}(2\pi+qa)$$
$$+\tfrac{1}{2}\,\mathrm{Si}(2\pi-qa)+\alpha\pi^2[j_1(qa)$$
$$-\tfrac{1}{2}j_1(2\pi+qa)+\tfrac{1}{2}j_1(2\pi-qa)]\}, \tag{15}$$
$$\langle r^2\rangle^{\frac{1}{2}}=\left[\frac{(2.79+15.26\alpha)^{\frac{1}{2}}}{\pi^2(1+2.79\alpha)}\right]a,$$

where $\mathrm{Si}(qa)=\int_0^{qa}(1/x)\sin x\,dx$ is the sine integral[20] and $j_1(qa)=\sin(qa)/(qa)^2-\cos(qa)/qa$ is the spherical Bessel function of order one. This is similar to the charge distribution obtained from shell-theory calculations using an infinite square well nuclear potential. A fit between theory and experiment was obtained for $\alpha=0.0$ and $\alpha=0.1$, as is shown in Fig. 6. The agreement here is not as good as for the modified Gaussian model,

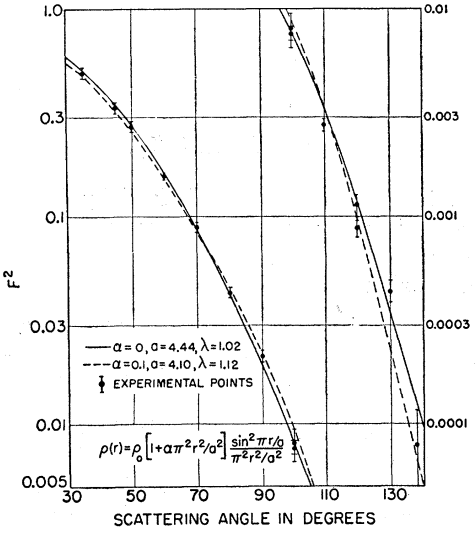

FIG. 5. Comparison of the square of the experimental form factor with the squares of the form factors for the modified Gaussian models; λ is the scale factor.

[19] D. G. Ravenhall (private communication).

[20] Tabulated in, e.g., *Tables of Sine, Cosine and Exponential Integrals* (Federal Works Agency, Work Projects Administration, New York, 1940).

and in the case of $\alpha=0.1$, the experimental values are about 11% less than the theoretical curve. This is barely within the error in absolute value which might be expected.

The third of Ravenhall's models, one with a long (exponential) tail in contrast to the two previous models, is

$$\rho(r)=\rho_0(1+r/a+\alpha r^2/a^2)e^{-r/a},$$
$$F(a)=\left(1+\frac{1-3\alpha}{1+3\alpha}q^2a^2\right)(1+q^2a^2)^{-4}, \tag{16}$$
$$\langle r^2\rangle=\left[18\frac{(1+5\alpha)}{(1+3\alpha)}\right]^{\frac{1}{2}}a.$$

This model can be made to fit the experimental results only with $-3<\alpha<\frac{1}{2}$. These values of α require a negative charge at the center of the nucleus and a corresponding increase in positive charge near the surface. Since such a charge distribution seems very unreal, this model was rejected.

The trapezoidal model of Hahn *et al.*[13] was also considered:

$$\rho(r)=\rho_0, \quad r<a,$$
$$=\rho_0\frac{(b-r)}{(b-a)}, \quad a<r<b,$$
$$=0, \quad r>b;$$
$$F(q)=\frac{12}{q^4b^4(1-a^4b^4)}(qa\sin qa-qb\sin qb+2\cos qa-2\cos qb); \tag{17}$$
$$\langle r^2\rangle^{\frac{1}{2}}=\left[\frac{2(1-a^6/b^6)}{5(1-a^4/b^4)}\right]^{\frac{1}{2}}b.$$

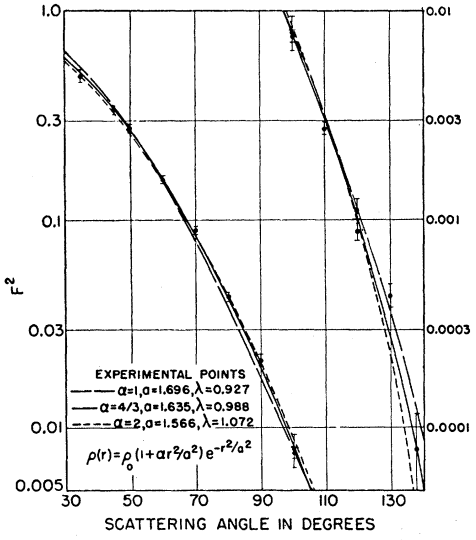

FIG. 6. Comparison of the square of the experimental form factor with the squares of the form factors for the modified trigonometric models; λ is the scale factor.

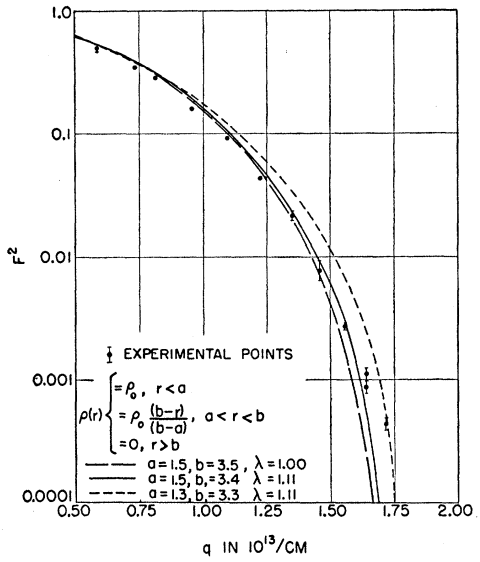

FIG. 7. Comparison of the square of the experimental form factor with the squares of the form factors for the trapezoidal models; λ is the scale factor.

A comparison of theory with experiment for three sets of parameters is shown in Fig. 7. While the fit is not good, it appears probable that a good fit could be obtained by determining the correct choice of values for a and b, but the new information that would be gained by this would not justify the large amount of labor required.

The three modified Gaussian charge distributions used are shown in Fig. 8, and the two modified trigonometric distributions in Fig. 9. The densities are plotted in proton charges/$(10^{-13}$ cm$)^3$ and the radii in 10^{-13} cm. The five distributions differ only slightly for radii greater than 1.3×10^{-13} cm. The radical differences in the central charge densities of five models are not

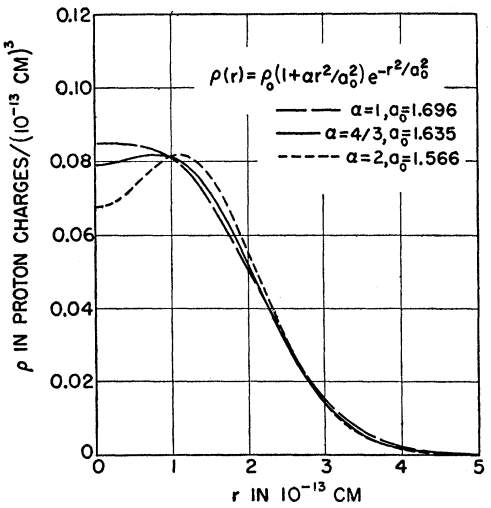

FIG. 8. Modified Gaussian charge distributions.

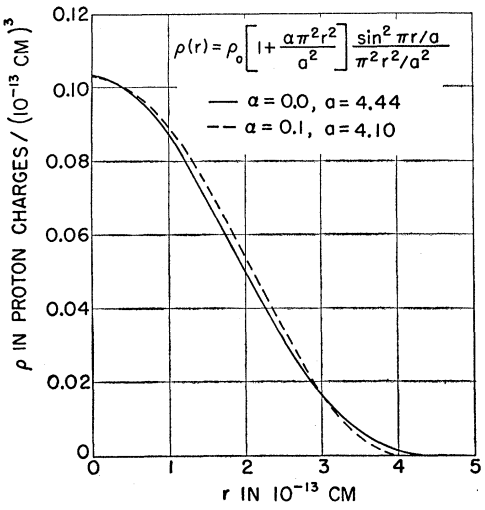

FIG. 9. Modified trigonometric charge distributions.

significant because the amount of charge at the center of the nucleus is small. This may be seen from Figs. 10 and 11, where the amount of charge at a given radius is plotted as a function of radius. Up to a radius of 1.3×10^{-13} cm there is virtually no difference between the five curves.

Figures 12 and 13 show the charge distribution and the amount of charge at a given radius, respectively, for the trapezoidal models. Since none of the models fits the experimental data, comparisons with the other models are not too meaningful. It is seen, however, that there is little difference between the amounts of charge at small radial distances in any of the cases.

The two radial parameters most frequently used are the root-mean-square radius of the charge distribution [Eq. (7)] and r_0 which is the radius of a uniform charge distribution having the same rms radius as the model considered, divided by the cube-root of the atomic number,

$$r_0=(5.3)^{\frac{1}{2}}\langle r^2\rangle^{\frac{1}{2}}A^{-\frac{1}{3}}. \tag{18}$$

The values of these constants which were found from the various models are given in Table II. Also shown in the table are the values of t, the distance in which the charge density drops from 0.9 to 0.1 of its maximum value and the values of the scale factor λ needed for the best agreement of each model with experiment. Disregarding the trapezoidal models, which do not fit the experimental data, the $\langle r^2\rangle^{\frac{1}{2}}$ and r_0 values have a maximum spread of about 4% around the values obtained from the modified Gaussian model with $\alpha=4/3$. This model also gives the best agreement with experiment for both the relative values as a function of angle and the absolute values. The values of the radial parameters thus determined are $\langle r^2\rangle^{\frac{1}{2}}=(2.37\pm0.05)\times10^{-13}$ cm and $r_0=(1.33\pm0.03)\times10^{-13}$ cm after the correction to the Born approximation has been made. This rms radius can be compared with the value $(2.75\pm0.05)\times10^{-13}$ cm for the rms radii of Li^6 and Li^7 determined by Streib.[21] It is also in good agreement with the value $(2.40\times0.20)\times10^{-13}$ cm for the nuclei from Li^6 to O^{16} calculated by Visscher and Ferrell,[16] using shell-model theory, harmonic well wave functions, and experimentally determined Coulomb energy differences. The value of r_0 found is about 10% larger than the value 1.25×10^{-13} cm found by Hahn *et al.*[13] for heavier elements and somewhat larger than the results obtained by Hahn *et al.* for calcium and by Helm[12] for the

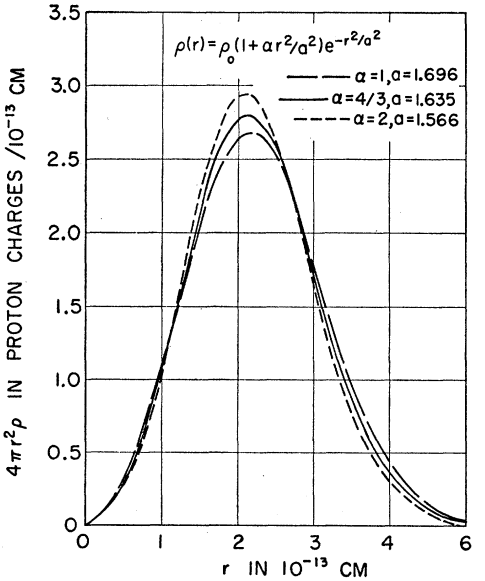

FIG. 10. Amount of charge at a given radius as a function of radius for the modified Gaussian models.

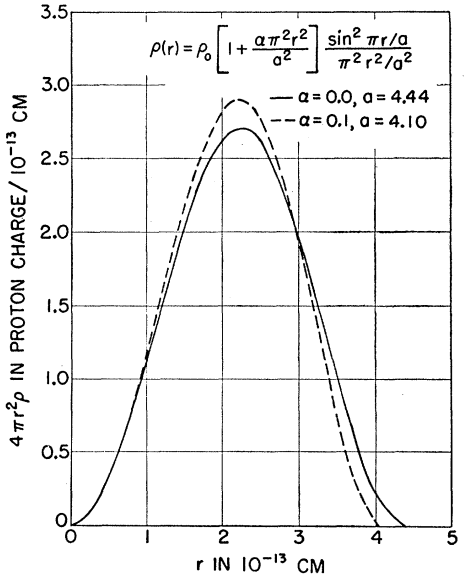

FIG. 11. Amount of charge at a given radius as a function of radius for the modified trigonometric models.

[21] J. F. Streib (private communication to R. Hofstadter); the results in an earlier report have been modified.

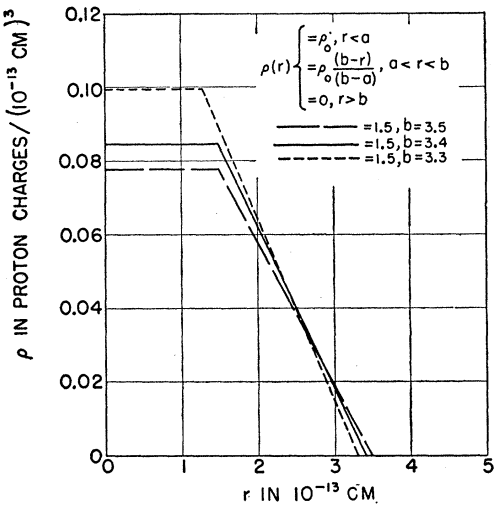

FIG. 12. Trapezoidal charge distributions.

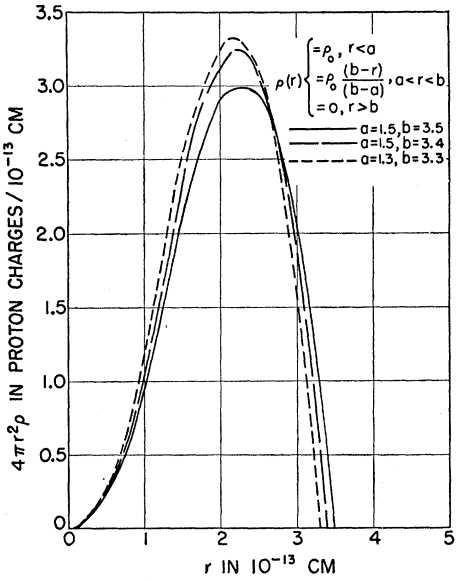

FIG. 13. Amount of charge at a given radius as a function of radius for the trapezoidal model.

intermediate elements. It is smaller than the value (about 1.90×10^{-13} cm) found by Streib.[21] It appears, therefore, that r_0 increases as the atomic number decreases, although local variations are possible.

The surface thickness parameter t shows considerable variation from model to model as would be expected since the maximum values for the change densities occur at radii less than 1.3×10^{-13} cm. Because very little about the charge distribution can be determined in this region, not much significance can be attached to the value of t, which is $(2.0\pm0.4)\times10^{-13}$ cm. The thickness appears to be less than the value $(2.4\pm0.3)\times10^{-13}$ cm found for the intermediate and heavy nuclei. The central charge densities of these models are slightly larger than those found for the larger nuclei.

B. Inelastic Scattering

The shell-model calculations of Ravenhall[2] and Morpurgo[3] have yielded predictions for the cross sections for inelastic scattering with excitation of the 4.43-Mev level. The nuclear potentials used were the infinite harmonic well,[2,3] the infinite square well,[2] and the infinite linear well.[2] The assumption of an infinite well simplified the calculations, but cannot be expected to apply at large angles because of large momentum transfers from the scattered electrons to the nuclei. The configuration assumed was $(1s)^4(1p)^8$. In each case, there are two parameters which can be adjusted when comparing theory with experiment. These are a radial parameter and the scale factor, both of which are the same for elastic and inelastic scattering. Both parameters are fixed by making the best possible fit between the theoretical and experimental elastic cross sections. The theoretical inelastic cross section is then completely determined.

A comparison of theory with experiment is shown in Fig. 14. Agreement can be obtained between the elastic scattering data and the theory up to 90° with

TABLE II. Radial and other parameters of the various models. All lengths in units of 10^{-13} cm; $\langle r^2\rangle^{\frac{1}{2}}$ is the root-mean-square radius, $r_0=(5/3)\langle r^2\rangle^{\frac{1}{2}}A^{-\frac{1}{3}}$; t is the thickness from 0.9 to 0.1 of the maximum value of the charge density; λ is the scale factor.

Model	Parameters	Uncorrected $\langle r^2\rangle^{\frac{1}{2}}$	Uncorrected r_0	Uncorrected t	λ	Corrected[a] $\langle r^2\rangle^{\frac{1}{2}}$	Corrected[a] r_0	Corrected[a] t
Modified Gaussian	$\alpha=1$, $a=1.696$	2.46	1.39	2.12	0.927	2.43	1.37	2.09
	$\alpha=4/3$, $a=1.635$	2.40	1.35	1.91	0.988	2.37	1.33	1.88
	$\alpha=2$, $a=1.566$	2.35	1.32	1.72	1.072	2.32	1.30	1.70
Modified trigonometric	$\alpha=0.0$, $a=4.44$	2.36	1.33	2.49	1.02	2.33	1.31	2.46
	$\alpha=0.1$, $a=4.10$	2.40	1.35	2.38	1.12	2.37	1.33	2.35
Trapezoidal (does not fit data)	$\alpha=1.5$, $b=3.5$	2.30	1.30	1.60	1.00	2.27	1.28	1.58
	$\alpha=1.5$, $b=3.4$	2.23	1.26	1.52	1.11	2.20	1.24	1.50
	$\alpha=1.3$, $b=3.3$	2.14	1.21	1.60	1.11	2.11	1.19	1.58

[a] Corrected for breakdown of the Born approximation. (See Sec. III.)

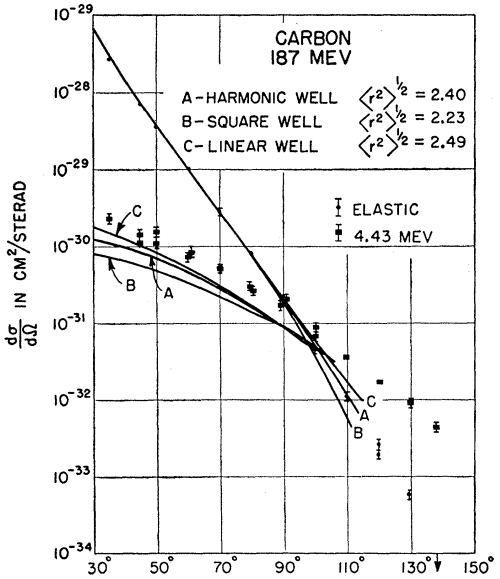

FIG. 14. Comparison of experimental cross sections with Ravenhall's shell-model calculations for elastic and inelastic (4.43 Mev) scattering. Scale factors and rms radii are chosen to fit the elastic data.

all three models if the following rms radii are chosen:

harmonic well $\langle r^2\rangle^{\frac{1}{2}}=2.40\times10^{-13}$ cm,
square well $\langle r^2\rangle^{\frac{1}{2}}=2.23\times10^{-13}$ cm,
linear well $\langle r^2\rangle^{\frac{1}{2}}=2.49\times10^{-13}$ cm.

The theoretical curves shown in Fig. 14 are those of Ravenhall.[2] The results obtained by Morpurgo[3] for the harmonic well are similar, but an rms radius of 2.23×10^{-13} cm was found using only the data previously published.[1] The value 2.40×10^{-13} cm is believed to be more accurate.

Beyond 90°, only the harmonic well result fits the data, but because of the assumption of an infinite well, this breakdown is not significant. It should be noted, however, that the rms radii required for the square and linear wells fall outside the limits of error placed on the value of this radius by the interpretation of the elastic scattering data given in the previous section.

In all three cases the predicted inelastic scattering is less than that found experimentally. The best agreement in angular dependence is found for the harmonic well, but this result is too small by a factor of two for $L-s$ coupling (shown in Fig. 14) and a factor of six for j-j coupling, assuming a single $(1p)$ particle excitation. Consideration of collective modes of excitation would probably remove this discrepancy since cross sections for collective excitations are in general an order of magnitude larger than those for single particle transitions.

A possible method for distinguishing between electric and magnetic transitions, which involves comparing cross sections at different energies, has been suggested by Ravenhall.[2,22] The cross section for electron scattering with magnetic excitation of the nucleus is a function of q only, while the ratios of the cross sections for scattering with electric excitation at the same q but different energies will be

$$\left(\frac{d\sigma}{d\Omega}\right)_{E_1}\Big/\left(\frac{d\sigma}{d\Omega}\right)_{E_2}=\frac{E_1^2\cos^2(\theta/2)}{E_2^2\cos^2(\theta/2)}. \tag{19}$$

Figure 15 shows the cross sections of the 4.43- and 9.61-Mev levels determined at 187 Mev compared with those cross sections at 150 Mev scaled electrically and magnetically. Figure 16 shows a similar result for the 7.65-Mev level. In all cases there is good agreement assuming electric scaling while magnetic scaling gives results which are too low by a factor of two. Since the transition to the 4.43-Mev level is believed to be electric monopole,[5] agreement with electric scaling is to be expected in these cases. A similar agreement, assuming electric scaling, is found in the elastic scattering at 80 Mev, 150 Mev, and 187 Mev, thus further demonstrating the validity of this analysis for the values of q involved. Figure 15 therefore suggests that the transition from the ground state to the 9.61-Mev level in C^{12} is electric.[2]

By expanding the general form of Eq. (25), reference 4, about $q=0$, the dependence of $F(q)$ upon q can be

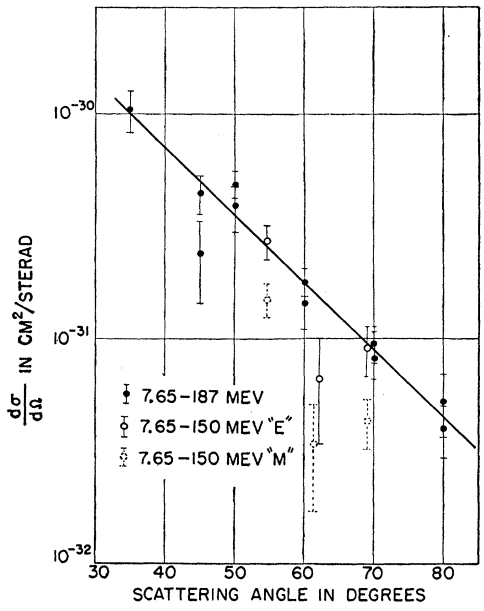

FIG. 15. Comparisons of electric "E" and magnetic "M" scaling for the 4.43 and 9.61-Mev cross sections. The 150-Mev cross sections are plotted for equivalent values of q. The cross sections for magnetic scaling are those found experimentally, while for electric scaling, the experimental cross sections were multiplied according to Eq. (19).

[22] D. G. Ravenhall, Phys. Rev. **100**, 1797(A) (1955).

found for values of q which are small compared to $1/\langle r^2\rangle^{\frac{1}{2}}$.

$$F(q)\propto q^l, \quad l\geq 2,$$
$$F(q)\propto q^3, \quad l=1, \quad T=0\rightarrow T=0, \qquad (20)$$
$$F(q)\propto q^2, \quad l=0,$$

where T is the isotopic spin and where l is the multipole order of the transition.[4] In the cases $l=0$ and $l=1$, the leading term of $F(q)$ vanishes due to the orthogonality of the initial and final nuclear states and the next higher term in the expansion is given in Eq. (20); it is found that only monopole and quadrupole electric transitions have cross sections which are finite for $q\cong 0$. The cross sections of all other transitions vanish at least as rapidly as q^2. The 9.61-Mev level cross section continues to increase as q is decreased, as do the cross sections for the 4.43-Mev level (quadrupole). This suggests that the 9.61-Mev transition is either monopole or quadrupole. Since in these cases no parity change takes place and the ground state is 0^+, the 9.61-Mev state must be either 0^+ or 2^+. The assignment 2^+ would agree with the prediction by Morinaga[23] based on the alpha-particle model for $4n$ self-conjugate nuclei. It may be noted that the 9.61-Mev cross section is similar to that of the 4.43-Mev (2^+) state and differs considerably from that of the 7.65-Mev (0^+) state. The possibility of a 4^+ assignment for the 9.61-Mev level, as suggested by Kurath,[24] appears to be ruled out as this would require the cross section to be proportional to q^4 at small angles.

Schiff[5] has shown that by using the ratios of the 7.65-Mev cross sections to the corresponding elastic cross sections as determined in this experiment, the size of the matrix element for the transition to the 7.65-Mev state may be determined. It is about 5×10^{-26} cm^2, with a probable error of about 25% due to statistical errors in the experiment and the fact that a considerable extrapolation from the present data is required. This is not in disagreement with the value 3.8×10^{-26} cm^2 quoted[5] for the ground state to 0^+ state transition in O^{16}. Schiff shows that both the elastic-fluid model and the alpha-particle model give values for this matrix element which are several times larger than the experimental value. He also shows that the independent-particle model, assuming j-j coupling and a two-nucleon transition from the $1p_{\frac{3}{2}}$ shell to the $1p_{\frac{1}{2}}$ shell gives a value about one-sixth of the experimental value. Schiff concludes that a model which is more collective than the independent-particle model and less collective than the alpha-particle or elastic-fluid models is required to account for the experimental results.

Recently, Elliott[17] and Redmond[18] have questioned Schiff's conclusion and suggested that an independent-particle model transition from the $1s$ shell to the $2s$ shell may give a matrix element of the required size. Elliott's calculation is for the O^{16} monopole transition and may not apply to C^{12} since the O^{16} lowest configuration, $(1s)^4(1p)^{12}$, is a closed shell, while the lowest configuration in C^{12}, $(1s)^4(1p)^8$, is not a closed shell, but has four holes. Redmond's calculations are for both C^{12} and O^{16}. The result for O^{16} gives a reasonable value for r_0. However, inserting the value fo r_0 determined by the present experiment into Eq. (6), reference 18 gives a value for the matrix element of 3.2×10^{-26} cm^2 which is close to, but somewhat smaller than the value 5×10^{-26} cm^2 experimentally found. Detailed calculations by Sherman and Ravenhall[6] using the $1p\rightarrow 2p$ transitions have also resulted in values of the matrix element which are too small to agree with this experiment.

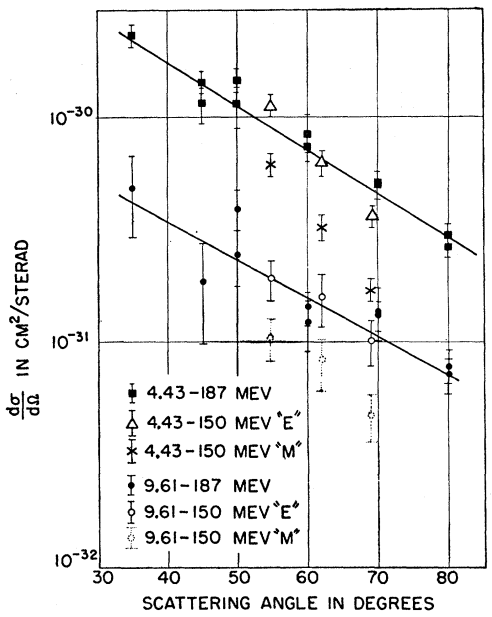

FIG. 16. Comparison of electric "E" and magnetic "M" scaling for the 7.65-Mev cross sections. The 150-Mev cross sections are plotted for equivalent values of q. The cross sections for magnetic scaling are those found experimentally, while for electric scaling, the experimental cross sections were multiplied according to Eq. (19).

Ravenhall[2] and Helm,[12] using data obtained in this experiment, have shown that the 4.43-Mev level has a transition width of 12.5 ± 2.5 mv, which corresponds to a mean lifetime for γ decay to the ground state of $(0.53\pm 0.11)\times 10^{-13}$ sec. Considering the large energy involved, compared with the 2^+ first excited states of other even-even nuclei, this is in reasonable agreement with Helm's other results.

IV. CONCLUSIONS

This experiment has shown that the root-mean-square radius of the C^{12} charge distribution is $(2.37\pm 0.05)\times 10^{-13}$ cm and that the surface thickness of the charge

[23] H. Morinaga, Phys. Rev. **101**, 254 (1956).
[24] D. Kurath, Phys. Rev. **101**, 216 (1956).

distribution is $(2.0\pm0.4)\times10^{-13}$ cm. Within the accuracy of the Born approximation, which is expected to be good for most carbon calculations, the independent-particle shell model using an infinite harmonic well has given the best agreement with experiment for the ground state and the first excited state scattering. An estimate of the size of the matrix element for the transition from the ground state to the 7.65-Mev state has been made. The transition to the 9.61-Mev level is probably electric and if this is the case, the possible spin and parity assignments for this state have been restricted to 0^+ and 2^+.

The author is especially indebted to Professor Robert Hofstadter, who suggested this project, for his help and advice throughout the work. I wish to thank Dr. D. G. Ravenhall for many helpful discussions and suggestions concerning the analysis of this experiment, and for making available formulas and calculations which have not yet been published. Thanks go to the operating and maintenance crews of the linear accelerator, whose efforts made possible this experiment; to the members of the electron scattering group, especially Professor Hofstadter, Dr. J. A. McIntyre, Dr. R. H. Helm, Lt. E. E. Chambers, A. W. Knudsen, and M. Yearian, for material assistance and discussion of the interpretation of the experimental data form this and other experiments; to B. Chambers and G. Signer for construction of the equipment and targets; and to Professor L. I. Schiff for discussion of some of the theoretical aspects of this work.

PHYSICAL REVIEW VOLUME 104, NUMBER 1 OCTOBER 1, 1956

Theory of S-Wave Pion Scattering and Photoproduction at Low Energies*†

S. D. DRELL,‡ M. H. FRIEDMAN, AND F. ZACHARIASEN§
Department of Physics and Laboratory for Nuclear Science, Massachusetts Institute of Technology, Cambridge, Massachusetts
(Received May 31, 1956)

A fixed-source analysis of the s-wave pion-nucleon interaction is constructed along the lines of the Chew-Low-Wick formalism. A bilinear s-wave interaction of the form $\lambda_0\boldsymbol{\varphi}\cdot\boldsymbol{\varphi}+\lambda\boldsymbol{\tau}\cdot(\boldsymbol{\varphi}\times\boldsymbol{\pi})$ is added to the usual p-wave coupling $(4\pi)^{\frac{1}{2}}(f/\mu)\boldsymbol{\sigma}\cdot\boldsymbol{\nabla}\,\boldsymbol{\tau}\cdot\boldsymbol{\varphi}$. Scattering equations are developed and solved in the one-meson approximation. Values for the renormalized coupling parameters λ_0 and λ are determined which give reasonable agreement with the s-wave phase shifts up to ~100-Mev pion kinetic energy. This s-wave interaction with the parameters fixed by the scattering analysis is then applied to the discussion of the π^+ and π^0 photo-production cross sections. A Kroll-Ruderman theorem is proved for the above nonlocal interaction and it is shown that the contributions to s-wave neutral and charged photoproduction are consistent with experiment. Other experimental implications, in particular as to the possible role of π-π forces, are discussed.

I. INTRODUCTION

CHEW and Low[1] have shown recently that a simple fixed-source theory of the p-wave pion-nucleon interaction is quite powerful in correlating low-energy pion scattering and photoproduction data. With a formalism based on a nonrelativistic approximation (which neglects antinucleons and recoil) to the equations of Low,[2,3] they have especially emphasized important conclusions in their work which are independent of the details of their model. We report here a fixed-source analysis of s-wave pion-nucleon interactions constructed along similar lines. In particular we study the elastic scattering of s-wave pions at low kinetic energy ($\leq$100 Mev) and the s-wave photoproduction of low-energy charged and neutral pions.

In C-L, the p-wave pion-nucleon coupling is taken to be

$$H_p'=(4\pi)^{\frac{1}{2}}\frac{f^0}{\mu}\int\{\boldsymbol{\sigma}\cdot\boldsymbol{\nabla}\boldsymbol{\tau}\cdot\boldsymbol{\varphi}(\mathbf{x})\}s(\mathbf{x})d^3\mathbf{x}, \qquad (1)$$

with a source density

$$s(\mathbf{x})=\int v(\boldsymbol{\kappa})\exp(i\boldsymbol{\kappa}\cdot\mathbf{x})\frac{d^3\boldsymbol{\kappa}}{(2\pi)^3}.$$

On the basis of Eq. (1) and in the "one-meson approximation" a low-energy effective-range theory of the p-wave scattering phase shifts is developed. The (3,3) phase shift ($T=\frac{3}{2}$, $J=\frac{3}{2}$) emerges as the dominant one.

* This work was supported in part by the Office of Naval Research and the U. S. Atomic Energy Commission.

† The term "pion" is used in discussion of the physical and experimental aspects of the scattering and photoproduction. In the more formal and theoretical developments we prefer the word "meson" for the nuclear field quantum. It is not intended that this duality of terms convey a basic reservation on our part as to the identity of these two.

‡ Now at the Physics Department, Stanford University, Stanford, California.

§ Now at the Physics Department, University of California, Berkeley, California.

[1] G. F. Chew and F. E. Low, Phys. Rev. **101**, 1570, 1579 (1956); hereafter referred to as C-L. We use the units $\hbar=c=1$. Unless specifically displayed, the pion rest mass $\mu=1$.

[2] F. E. Low, Phys. Rev. **97**, 1392 (1955).

[3] G. C. Wick, Revs. Modern Phys. **27**, 339 (1955).